

Azimuthally-integrated HBT parameters for charged pions in nuclear-nuclear collisions versus initial energy

V.A. Okorokov*

*National Research Nuclear University "MEPhI" (Moscow Engineering
Physics Institute), Kashirskoe Shosse 31, 115409 Moscow, Russia*

(Dated: September 9, 2014)

In the paper energy dependence of space-time extent of charged pion source is studied for various ion collisions for all experimentally available energies. There are no sharp changing of femtoscopy parameter values with increasing of $\sqrt{s_{NN}}$ in domain of collision energies $\sqrt{s_{NN}} \geq 5$ GeV. Energy dependence of estimations for emission duration is almost flat for all energy domain under study within large error bars. Analytic function is suggested for smooth approximation of energy dependence of main HBT parameters. Fit curves demonstrate reasonable agreement with experimental data for most femtoscopy parameters in energy domain $\sqrt{s_{NN}} \geq 5$ GeV. Estimations of femtoscopy observables are obtained for energies of the LHC and FCC project.

PACS 25.75.-q, 25.75.Gz, 25.75.Nq

I. INTRODUCTION

At present femtoscopy correlations in particular that based on Bose–Einstein correlations are unique experimental method for the determination of sizes and lifetimes of sources in high energy and nuclear physics. The discussion below is focused on specific case of femtoscopy, namely, on correlations in pairs of identical charged pions with small relative momenta – HBT-interferometry – in nuclear-nuclear collisions. Space-time characteristics for emission region of secondary particles created in (heavy) ion collisions are important for study of deconfinement state of strongly interacting matter – strong-coupling quark-gluon plasma (sQGP). Furthermore the study of energy dependence of femtoscopy observables can be useful for understanding in detail the transition from sQGP produced at higher energies to confined hadronic resonance matter created in final state at lower energies. HBT method allows to study dynamic features of interaction process at late, i.e. soft, stage of space-time evolution of multiparticle final state. Therefore the study of nuclear-nuclear collisions in wide energy domain by correlation femtoscopy seems important for better understanding both of equation of state (EOS) of strongly interacting matter and general dynamic features of soft processes.

The paper is organized as follows. In Sec.2, definitions of main observables for correlation femtoscopy are briefly described. The Sec.3 devotes discussion of experimental energy dependence for space-time extent of charged pion source and corresponding fits. Also estimations for femtoscopy observables are shown for the LHC and FCC project energies. Some final remarks and conclusions are presented in Sec.4.

II. METHOD AND VARIABLES

In general phenomenological parameterization of correlation function (CF) for two identical particles with 4-momenta p_1, p_2 and with taking into account different forms of corrections on Coulomb final state interaction (FSI) can be written as follows [1]:

$$C_{2,(m)}^{\text{ph}}(q, K) = \epsilon P_{\text{coul}}^{(m)}(q) [\epsilon^{-1} + \mathbf{K}_2^{\text{ph}}(\mathbf{A})], \quad \epsilon = \begin{cases} \lambda, & \text{at } m = 1, 2; \\ 1, & \text{at } m = 3. \end{cases} \quad (1)$$

where $m = 1$ corresponds to the standard Coulomb correction, $m = 2$ – dilution procedure and $m = 3$ – Bowler–Sinyukov correction, $q \equiv (q^0, \vec{q}) = p_1 - p_2$ is the relative 4-momentum, $K \equiv (K^0, \vec{K}) = (p_1 + p_2)/2$ – average 4-momentum of particles in pair (pair 4-momentum), for standard simplest (Gaussian) case

$$\mathbf{K}_2^{\text{ph}}(\mathbf{A}) = \prod_{i,j=1}^3 \mathbf{K}_2^{\text{ph}}(A_{ij}) = \exp\left(-\sum_{i,j=1}^3 q_i R_{ij}^2 q_j\right). \quad (2)$$

*Electronic address: VAOkorokov@mephi.ru; okorokov@bnl.gov

Here $\mathbf{A} \equiv \vec{q} \mathbf{R}^2 \vec{q}^T$ and \mathbf{R}^2 are the matrices 3×3 , \vec{q}^T – transposed vector \vec{q} , $\forall i, j : R_{ij}^2 = R_{ji}^2, R_{ii}^2 \equiv R_i^2$, where $R_i = R_i(K)$ are parameters characterized the linear scales of homogeneity region [2]; the products are taken on space components of vectors, $\lambda(K) = \mathbf{K}_2(0, K), 0 \leq \lambda \leq 1$ is the parameter which characterizes the degree of source chaoticity. Taking into account the hypothesis of cylindrical symmetry of source the volume of homogeneity region was derived as follows [3]

$$V = (2\pi)^{3/2} \prod_{i=1}^3 R_i. \quad (3)$$

The space component of pair 4-momentum (\vec{K}) is decomposed on longitudinal $k_{\parallel} = (p_{\parallel,1} + p_{\parallel,2})/2$ and transverse $\vec{k}_{\perp} = (\vec{p}_{\perp,1} + \vec{p}_{\perp,2})/2$ parts of pair momentum. In the paper decomposition of Pratt–Bertsch [4, 5] is used for \vec{q} as well as the longitudinal co-moving system (LCMS) frame. The radius R_o contains additional contribution from the temporal extent of the source. Therefore this parameter is usually excluded from calculation of V and the volume of source can be written as follows

$$V = (2\pi)^{3/2} R_s^2 R_l. \quad (4)$$

As seen $V^{(3)}/V^{(4)} = R_o/R_s$, where $V^{(3)}$ denotes the source volume calculated from eq. (3) and the volume of emission region defined in accordance with eq. (4) is designated by $V^{(4)}$. But it should be emphasized that in the limit for absolute value of transverse pair momentum vector $k_{\perp} \rightarrow 0$, no transverse vector allows to distinguish between out- and side-components [6, 7]. This implies that $\lim_{k_{\perp} \rightarrow 0} R_o(K) = \lim_{k_{\perp} \rightarrow 0} R_s(K)$. Consequently, it is expected $V^{(3)} \approx V^{(4)}$ for particles with low k_{\perp} and both relations (3) and (4) for freeze-out volume are valid for such particles.

The one of the important additional observable is the following difference [8, 9]

$$\delta \equiv R_o^2 - R_s^2. \quad (5)$$

If the emission function features no position-momentum correlation, then δ is finite at non-zero \vec{K} only due to explicit \vec{K} -dependence (resulting from the mass-shell constraint $q^0 = \vec{q}\vec{K}/K^0$) [6]. In this case

$$\delta \approx \beta_{\perp}^2 (\Delta\tau)^2, \quad (6)$$

where $\beta_{\perp} = k_{\perp}/m_{\perp}$ is the transverse velocity of pair of particles with mass m , $m_{\perp}^2 = k_{\perp}^2 + m^2$, $\Delta\tau$ – the emission duration for the particle type under discussion. It should be stressed the last relation is valid in some specific cases 1D hydrodynamics and violates in cascade models of multidimensional hydrodynamic models. Thus in the framework of some assumptions the δ gives direct access to the emission duration of the source and allows to partially disentangle the spatial and temporal information contained in radii parameters R_{ij} [6]. The sensitivity to the $\Delta\tau$ is the main advantage of the observable (5).

In the paper the following set of main femtoscopy observables $\mathcal{G}_1 \equiv \{\mathcal{G}_1^i\}_{i=1}^4 = \{\lambda, R_s, R_o, R_l\}$ is under consideration as well as the set of some important additional observables which can be calculated with help of HBT radii $\mathcal{G}_2 \equiv \{\mathcal{G}_2^j\}_{j=1}^3 = \{R_o/R_s, \Delta\tau, V\}$. The set of parameters \mathcal{G}_1 characterizes the chaoticity of source and its 4-dimensional geometry at freeze-out stage completely. Scaled femtoscopy parameters \mathcal{G}_1^i , $i = 2 - 4$, δ and \mathcal{G}_2^3 are calculated as follows [1]:

$$R_i^n = R_i/R_A, \quad i = s, o, l; \quad \delta^n = \delta/R_A^2; \quad V^n = V/V_A. \quad (7)$$

Here $R_A = r_0 A^{1/3}$, $V_A = 4\pi R_A^3/3$ is radius and volume of spherically-symmetrical nucleus, $r_0 = (1.25 \pm 0.05)$ fm [10, 11]. The change $R_A \rightarrow \langle R_A \rangle = 0.5(R_{A_1} + R_{A_2})$ is made in the relation (7) in the case of non-symmetrical nuclear-nuclear collisions [1]. One need to emphasize the most central collisions are usually used for study the space-time characteristics of final-state matter, in particular, for discussion of global energy dependence of femtoscopy observables (see below Sec. 3). Thus the using of radius of all nucleus in (7) seems reasonable. In general case the scale factor in (7) for calculation of normalized femtoscopy radii, δ and volume should takes into account the centrality of nuclear-nuclear collisions. The normalization procedure suggested in [1] allows to consider two data samples, namely, (i) only (quasi)symmetrical heavy ion collisions and (ii) all available data for nuclear-nuclear collisions. Ensemble of experimental data reviewed in [1] with replacement of Au+Au points at $\sqrt{s_{NN}} \geq 9.2$ GeV by the recent STAR results of high-statistics analysis for Au+Au collisions at $\sqrt{s_{NN}} = 7.7, 11.5 - 62.4$ and 200 GeV [12] are used in the present study.

III. ENERGY DEPENDENCE OF SPACE-TIME EXTENT OF PION SOURCE

Dependencies of femtoscopy parameters $\mathcal{G}_1^i(\sqrt{s_{NN}})$, $i = 1-4$ and $R_o/R_s(\sqrt{s_{NN}})$ are shown in Figs. 1a – d and Fig. 1e respectively. These results were obtained for fit function (2) with taking into account two additional cross-terms for R_{os} and R_{ol} as well as with improved Coulomb correction $P_{\text{coul}}^{(3)}(q)$. The two sets of STAR results for $\{\mathcal{G}_1^i\}_{i=1}^4$ are in a good agreement for previously study [1] and for present analysis for most femtoscopy parameters under consideration in Fig. 1. The some decreasing is seen for λ and transverse radii R_o , R_s for Au+Au collisions at $\sqrt{s_{NN}} = 200$ GeV with respect to the earlier STAR results from [13]. The new results from [12] agree better both with general trends and with results of other experiments (PHENIX and PHOBOS) at top RHIC energy $\sqrt{s_{NN}} = 200$ GeV. The chaoticity parameter λ decreases with increasing $\sqrt{s_{NN}}$ relatively rapidly at lower (AGS) energies and shows the weak changing at $\sqrt{s_{NN}} > 4$ GeV (Fig. 1a). Femtoscopy radii of source in transverse plane with respect to the beam direction, R_s (Fig. 1b) and R_o (Fig. 1c), show little change over a wide range of energy $5 \lesssim \sqrt{s_{NN}} \lesssim 200$ GeV which corresponds to highest AGS – SPS – RHIC beam collision energies. On the other hand, the values of source size in longitudinal direction, R_l (Fig. 1d), appear to reach a minimum around $\sqrt{s_{NN}} = 5$ GeV, rising in energy domain available at RHIC. As seen there is increasing of HBT radii (Figs. 1b – d) at growth of collision energy from $\sqrt{s_{NN}} \sim 20$ GeV up to maximum available LHC energy $\sqrt{s_{NN}} = 2.76$ TeV. The significant increasing of HBT radii is seen for much broader energy range (on about two order of magnitude $\sqrt{s_{NN}} \sim 0.02 - 3$ TeV) only than it was expected early at the beginning of RHIC operation. Therefore the space-time extent of emission region at freeze-out changes slowly at increasing of collision energy. The transverse radius R_s reflects the spatial extent of particle source, whereas R_o is also affected by dynamics [14, 15] and is believed to be related to the duration of particle emission [8]. As indicated, for example, in [12], the ratio R_o/R_s was predicted to increase with beam energy by hydrodynamical calculations and might show an significant enhancement if the life-time of the collision evolution (and, within these models, the duration of particle emission as a result) were to be extended by entrance into a different phase [8]. There is no significant increasing of ratio R_o/R_s in all experimentally available energy domain (Fig. 1e). Recent developments, in particular in viscous hydrodynamics, allow to get reasonable agreement between experimental and model values of R_o/R_s at top RHIC energy and demonstrate that the behavior of experimental dependencies of R_o/R_s on kinematic variables can be explained in particular by realistic EoS with crossover phase transition and sQGP at high temperatures [16–21]. Therefore the soft femtoscopy observables confirm the phase transition and creation of deconfinement state of strongly interacting matter in collider experiments.

Taking into account the view of the experimental dependencies in Figs. 1a – d the following function is suggested

$$f(\sqrt{s_{NN}}) = a_1 [1 + a_2(\ln \varepsilon)^{a_3}] \quad (8)$$

for smooth approximation of $\mathcal{G}_1^i(\sqrt{s_{NN}})$, $i = 1 - 4$, where $\varepsilon \equiv s_{NN}/s_0$, $s_0 = 1 \text{ GeV}^2$. Also the specific case of (8) at $a_3 = 1.0$ is under consideration. As seen from Figs. 1b – d there is indication on changing of behavior of energy dependence (inflection point) for $\{\mathcal{G}_1^i\}_{i=2}^4$ at $\sqrt{s_{NN}} \simeq 5$ GeV. This inflection point is seen most clear for R_l (Fig. 1d). Therefore the fit function (8) is used for approximation of energy dependence of HBT radii in energy domain $\sqrt{s_{NN}} \geq 5$ GeV only. Experimental energy dependence of λ is fitted by general function (8) at all available energy. As seen the point from the WA97 experiment [22] differs significantly from other results at close energies for λ (Fig. 1a) and longitudinal radius (Fig. 1d). Thus for these parameters fits were made for data sample (i) with exception of the point from [22]. For each main HBT parameters $\{\mathcal{G}_1^i\}_{i=1}^4$ fits were made both for statistical and for total errors, where total errors of experimental points include available clear indicated systematic errors added in quadrature to statistical ones. The numerical values of fit parameters are presented in Table I, where the second line for each HBT parameter $\{\mathcal{G}_1^i\}_{i=1}^4$ corresponds to the approximation by specific case of (8). Fit curves are shown in Fig. 1 by solid lines for (8) and by dashed lines for specific case of fit function at $a_3 = 1.0$ with taking into account the statistical errors. In general fit function described above agrees quantitatively with experimental dependence $\mathcal{G}_1^i(\sqrt{s_{NN}})$, $i = 1 - 4$ (Fig. 1a – d). But the fit qualities are poor for all main HBT parameters, especially for λ , with statistical error taken into account (Table I). Spread of experimental points leads to the statistically unacceptable values of $\chi^2/\text{n.d.f.}$. Account for total errors allows to get a statistically acceptable fit qualities for HBT radii for both function (8) and its specific case. It seems more complex fit function should be used in order to describe energy dependence of HBT radii at all available collision energies. This study is in the progress. Taking into account the similar behavior of energy dependence of HBT radii (Figs. 2b – d) and elliptic flow v_2 [23] at qualitative level the following functional form can be suggested $g(\sqrt{s_{NN}}) = a_1 + a_2(\sqrt{\varepsilon} - a_3)^{a_4} + \sum_{i=5,6} a_i \varepsilon^{a_i+1} + a_9(\ln \varepsilon)^{a_{10}}$ as first approach for description of $\mathcal{G}_1^i(\sqrt{s_{NN}})$, $i = 1 - 4$ in all experimentally available energy domain. Smooth solid and dashed curves shown in Fig. 1e were calculated for the ratio R_o/R_s from fit results for R_s and R_o (Table I). As seen these curves agree with experimental points reasonably at $\sqrt{s_{NN}} \geq 5$ GeV. In general fits by the function (8) at free a_3 and fixed a_3 show close behavior for all main HBT parameters from \mathcal{G}_1 with some differences at intermediate ($\sqrt{s_{NN}} \lesssim 10$ GeV) and high ($\sqrt{s_{NN}} > 200$ GeV) energies. These differences result in more significant discrepancy between fit curves for R_o/R_s (Fig. 2e) and for other parameters from the set \mathcal{G}_2 (see below).

TABLE I: Values of fit parameters for approximation of data sample (i)

HBT parameter	Fit with statistical errors				Fit with total errors			
	a_1	a_2	a_3	$\chi^2/\text{n.d.f.}$	a_1	a_2	a_3	$\chi^2/\text{n.d.f.}$
λ	0.36 ± 0.02	1.90 ± 0.12	-0.91 ± 0.14	534/23	0.008 ± 0.002	104 ± 21	-0.291 ± 0.011	373/23
	0.570 ± 0.004	-0.021 ± 0.001	1.0 (fixed)	580/19	0.621 ± 0.005	-0.032 ± 0.001	1.0 (fixed)	266/19
R_s	4.77 ± 0.02	$(1.3 \pm 0.8) \times 10^{-4}$	2.8 ± 0.2	141/22	4.5 ± 0.2	$(1 \pm 2) \times 10^{-3}$	2.3 ± 0.9	51.1/22
	4.37 ± 0.03	0.0188 ± 0.0012	1.0 (fixed)	194/23	3.88 ± 0.18	0.038 ± 0.008	1.0 (fixed)	54.5/23
R_o	0.59 ± 0.06	7.4 ± 1.0	0.097 ± 0.009	392/22	0.64 ± 0.11	7 ± 2	0.03 ± 0.03	31.9/22
	5.38 ± 0.04	0.0120 ± 0.0012	1.0 (fixed)	411/23	5.3 ± 0.2	0.003 ± 0.002	1.0 (fixed)	31.9/23
R_l	0.110 ± 0.015	32 ± 4	0.267 ± 0.008	357/21	0.03 ± 0.03	87 ± 64	0.33 ± 0.03	23.3/21
	4.51 ± 0.04	0.0475 ± 0.0018	1.0 (fixed)	459/22	4.0 ± 0.2	0.065 ± 0.010	1.0 (fixed)	26.3/22

Fig. 2 demonstrates the energy dependence of $\Delta\tau$ for (quasi)symmetrical heavy ion collisions. The emission duration in these collisions is calculated based on known HBT-radii (Figs. 1b – d), kinematic regime for pion pairs and on (6). The $\langle\beta_\perp\rangle \approx 0.82$ for pion pairs with $\langle k_\perp\rangle \simeq 0.2$ GeV/c. Value $\Delta\tau = (0.53 \pm 9.15)$ fm/c at $\sqrt{s_{NN}} = 130$ GeV derived from PHENIX results at this energy is not shown due to extremely large errors. As seen the emission duration of pion source is about 2 – 4 fm/c for any energies under consideration. The visible energy dependence of emission duration is absent, $\Delta\tau(\sqrt{s_{NN}})$ is close to flat within large error bars. One can see more interesting behavior for this dependence for STAR high-statistics data [12] only. But additional precise measurements are necessary in order to confirm the change of $\Delta\tau(\sqrt{s_{NN}})$ at $\sqrt{s_{NN}} \sim 10 - 20$ GeV and locate the possible knee in the experimental dependence. Smooth solid and dashed curves shown in Fig. 2 were calculated for $\Delta\tau$ from fit results for R_s and R_o (Table I). It seems the function (8) at free a_3 agrees better with experimental points at $\sqrt{s_{NN}} \leq 200$ GeV than that at fixed a_3 . But large error bars do not allow to choice preferable curve unambiguously. Moreover the general function (8) underestimates $\Delta\tau$ in TeV-region significantly.

The volume of homogeneity region in various heavy ion collisions is calculated based on known HBT-radii which were shown in Figs. 1b – d. Both equations (3) and (4) are used for verification and increasing of reliability of results. The first approach is the same as in the previous study [1]. As expected the values of V are similar for both equations (3) and (4) that it confirms the validity of the results from [1]. The energy dependence of estimations of emission region volume from (4) is shown in Fig. 3. It would be emphasized that values of V calculated at $\sqrt{s_{NN}} = 62.4$ and 200 GeV from recent STAR high-statistics results [12] agree better, especially at top RHIC energy, with results of other experiments (PHENIX and PHOBOS) than that in earlier study [1]. The values of $V^{(3)}$ which are derived here from STAR results obtained in the framework of the phase-I beam energy program (BES) at RHIC in energy domain $\sqrt{s_{NN}} = 7.7 - 39$ GeV form the trend lies some higher than the most of results from AGS and SPS. But on the other hand the spread of results at $\sqrt{s_{NN}} = 7 - 20$ GeV is within total errors if systematic uncertainties will be taken into account also. The values of $V^{(4)}$ from STAR results at energies $\sqrt{s_{NN}} = 7.7 - 39$ GeV [12] agree noticeably better with AGS and SPS results (Fig. 3) than that for $V^{(3)}$. Results for volume at $\sqrt{s_{NN}} = 7.7 - 39$ GeV which are derived from STAR high-statistics data [12] based on (3) as well as on (4) agree better with (quasi)linear growth V with $\ln \epsilon$ from $\sqrt{s_{NN}} \simeq 5$ GeV up to highest RHIC energy than that the earlier data at close energies. Smooth solid and dashed curves shown in Fig. 3 were calculated for V from equation (4) and fit results for R_s , R_l (Table I). Both curves are very close at $\sqrt{s_{NN}} \leq 200$ GeV but function (8) at $a_3 = 1.0$ underestimates $V^{(6)}$ in TeV-region significantly. Therefore the general function (8) is the preferable approximation of the experimental $V^{(6)}(\sqrt{s_{NN}})$ at $\sqrt{s_{NN}} \geq 5$ GeV.

Predictions for values of femtoscopy observables from sets \mathcal{G}_m , $m = 1, 2$ were obtained for the LHC design energy and for FCC project based on the fit results for main HBT parameters. Estimations are shown in Table II for fits with account for statistical errors, the second line for each collision energy corresponds to the using of the specific case of (8), the volume of homogeneity region is estimated with help of (4). The large uncertainties obtained for estimations based on the function (8) do not allow to distinguish predictions from (8) with free a_3 and with fixed $a_3 = 1.0$. One can expect the volume of homogeneity region $V^{(4)} \sim 6000$ fm³ at $\sqrt{s_{NN}} = 5.52$ TeV (LHC) and $V^{(4)} \sim 9000$ fm³ at $\sqrt{s_{NN}} = 39.0$ TeV (FCC) based on the reasonable agreement between experimental data and solid curve at Fig. 3.

Fig. 4 shows the energy dependence of λ (a), scaled HBT-radii (b – d) and R_o/R_s ratio (e) both for symmetrical and non-symmetrical collisions of various nuclei. Fits of experimental dependencies for data sample (ii) were made by (8) in the same energy domains and with same error types as well as for data sample (i) above. It seems the λ value from WA97 experiment [22] can not be excluded from the data sample (ii) because there are STAR results $\lambda \sim 0.3$

TABLE II: Estimations for observables based on fit results for the data sample (i)

$\sqrt{s_{NN}}$, TeV	HBT parameter						
	λ	R_s , fm	R_o , fm	R_l , fm	R_o/R_s	$\Delta\tau$, fm/c	$V \times 10^{-3}$, fm ³
5.52	0.41 ± 0.03	6.8 ± 1.9	6.3 ± 1.0	7.6 ± 1.5	0.9 ± 0.3	–	6 ± 3
	0.362 ± 0.009	5.79 ± 0.10	6.49 ± 0.12	8.20 ± 0.16	1.12 ± 0.03	3.6 ± 0.4	4.33 ± 0.17
39.0	0.40 ± 0.02	8 ± 3	6.4 ± 1.0	8.0 ± 1.6	0.8 ± 0.3	–	9 ± 8
	0.315 ± 0.011	6.11 ± 0.12	6.74 ± 0.15	9.04 ± 0.19	1.10 ± 0.03	3.5 ± 0.5	5.3 ± 0.2

for Cu+Cu collisions also (Fig. 4a). There are no physics reasons in order to exclude the points of these experiments from the fitted data sample (ii) in the case of all available nuclear-nuclear collisions. Furthermore the scaled value of longitudinal radius R_l^n from [22] agrees better with results of other experiments at close energies (Fig. 4d) than that for data sample (i). Therefore there is no exception of any experimental point from fitted ensemble for any HBT observable in Fig. 4 in contrast with the fitting procedure for data sample (i). The numerical values of fit parameters are presented in Table III, where the second line for λ and each normalized HBT radius corresponds to the approximation by specific case of (8). Fit curves are shown in Fig. 4 by solid lines for (8) and by dashed lines for specific case of fit function at $a_3 = 1.0$ with taking into account the statistical errors. Fit qualities improved for R_s^n in the case of total errors of experimental point and for R_o^n at any error types of experimental point with respect to the corresponding fits for data sample (i) shown in Table I. There is dramatic growth of $\chi^2/\text{n.d.f.}$ values for fits of λ data (Fig. 4a) despite of qualitative agreement between smooth approximations and experimental λ values for range $10 \lesssim \sqrt{s_{NN}} \lesssim 200$ GeV. The fit by (8) at $a_3 = 1.0$ underestimates λ value at the LHC energy $\sqrt{s_{NN}} = 2.76$ TeV significantly. The λ values for asymmetrical nuclear-nuclear collisions at intermediate energies $\sqrt{s_{NN}} \lesssim 20$ GeV agree well with values of λ in symmetrical heavy ion collisions at close energies. On the other hand the λ for Cu+Cu collisions is smaller systematically than λ in Au+Au collisions in energy range $\sqrt{s_{NN}} = 62 - 200$ GeV (Fig. 4a). New experimental data are important for verification of the suggestion of separate dependencies $\lambda(\sqrt{s_{NN}})$ for moderate and heavy ion collisions. Also the development of some approach is required in order to account for type of colliding beams in the case of λ parameter and improve quality of smooth approximation. Smooth curves for normalized HBT radii and ratio R_o/R_s are in reasonable agreement with experimental dependencies in fitted domain of collision energies $\sqrt{s_{NN}} \geq 5$ GeV (Figs. 4b – e). Parameter values obtained for fit of R_l^n with total uncertainties by (8) at $a_3 = 1.0$ are equal within errors with results from [24] accounting for that experimental results studied here were obtained at $\langle m_\perp \rangle \simeq 1.75m_\pi$.

TABLE III: Values of fit parameters for approximation of data sample (ii)

HBT parameter	Fit with statistical errors				Fit with total errors			
	a_1	a_2	a_3	$\chi^2/\text{n.d.f.}$	a_1	a_2	a_3	$\chi^2/\text{n.d.f.}$
λ	$(3.9 \pm 0.4) \times 10^{-4}$	4100 ± 400	-0.655 ± 0.005	4298/29	0.005 ± 0.001	160 ± 29	-0.31 ± 0.01	859/29
	0.717 ± 0.003	-0.051 ± 0.001	1.0 (fixed)	3786/23	0.631 ± 0.005	-0.034 ± 0.001	1.0 (fixed)	706/23
R_s^n	0.656 ± 0.002	$(6 \pm 3) \times 10^{-5}$	3.11 ± 0.19	195/25	0.63 ± 0.02	$(6 \pm 5) \times 10^{-4}$	2.4 ± 0.9	26.8/25
	0.599 ± 0.003	0.019 ± 0.001	1.0 (fixed)	280/26	0.56 ± 0.03	0.029 ± 0.008	1.0 (fixed)	28.9/26
R_o^n	0.10 ± 0.02	6.3 ± 1.7	0.068 ± 0.006	402/25	0.019 ± 0.003	30 ± 9	0.12 ± 0.05	23.9/25
	0.758 ± 0.004	0.008 ± 0.001	1.0 (fixed)	415/26	0.67 ± 0.04	0.017 ± 0.008	1.0 (fixed)	24.4/26
R_l^n	0.022 ± 0.002	23 ± 3	0.258 ± 0.005	502/25	0.23 ± 0.04	0.8 ± 0.2	0.57 ± 0.05	66.0/25
	0.634 ± 0.004	0.043 ± 0.001	1.0 (fixed)	615/26	0.47 ± 0.03	0.089 ± 0.014	1.0 (fixed)	66.7/26

The corresponding dependencies for δ^n and V^n are demonstrated in Fig. 5 and Fig. 6, respectively. The definition (4) for source volume is used in Fig. 6 as well as in Fig. 3 above. As well as in [1] the results for $\pi^+\pi^+$ pairs are shown in Figs. 4 – 6 also because femtoscopy parameters from the set \mathcal{G}_1 depend on sign of electrical charge of secondary pions weakly. The relation $R_o < R_s$ is observed for $\approx 11\%$ of points in Fig. 5. In general the $\delta < 0$ can be possible in the model of opaque source with surface dominated emission [25, 26]. But possibly results should be similar for both same ion beams and close kinematic regimes in various experiments. Therefore additional study is

requested in order to distinguish the physical and technique sources of negative values of δ^n in Fig. 5 and to get a more definite explanation. The dependence $\delta^n(\sqrt{s_{NN}})$ is almost flat within large error bars in all energy domain under consideration. Taking into account the STAR high-statistics results [12] only one can see the indication on change of behavior of $\delta^n(\sqrt{s_{NN}})$ inside the range of collision energy $\sqrt{s_{NN}} = 11.5 - 19.6$ GeV. This observation is in agreement with features of behavior of emission duration dependence on $\sqrt{s_{NN}}$ (Fig. 2) discussed above. The estimation of energy range agrees well with results of several studies [12, 27–32] in the framework of phase-I of beam energy scan program at RHIC which indicate on the transition from dominance of quark-gluon degrees of freedom to hadronic matter at $\sqrt{s_{NN}} \lesssim 19.6$ GeV. But future precise measurements are crucially important for extraction of more definite physics conclusions. Smooth solid and dashed curves shown in Fig. 5 were calculated for δ^n from fit results for R_s^n and R_o^n (Table III). The situation is similar to that for $\Delta\tau$: calculation based on the fit function (8) at free a_3 agrees reasonably with experimental points at $\sqrt{s_{NN}} \leq 200$ GeV but underestimates δ^n in TeV-region significantly. The large errors in Fig. 6 for strongly non-symmetrical nuclear collisions is dominated by large difference of radii of colliding moderate and heavy nuclei and corresponding large uncertainty for $\langle R_A \rangle$. Smooth solid and dashed curves shown in Fig. 6 were calculated for V^n from equation (4) and fit results for R_s^n , R_l^n (Table III). The fit results for normalized HBT radii obtained with general function (8) lead to very good agreement between smooth curve and experimental data in TeV-region in contrast with the curve obtained from corresponding fit results for (8) at $a_3 = 1.0$.

Estimations for λ , R_o/R_s , and normalized femtoscopy parameters at the LHC and FCC energies are shown in Table IV for fits of various nuclear-nuclear collisions with account for statistical errors, the second line for each collision energy corresponds to the using of the specific case of (8) at $a_3 = 1.0$, the volume of homogeneity region is estimated with help of (4). All smooth approximation discussed above predict amplification of coherent pion emission with significant decreasing of λ , especially, in the case of linear function on $\ln \varepsilon$. Uncertainties are large for estimations obtained on the basis of results of fits by function (8) at free a_3 . Thus values of femtoscopy observables in Table IV are equal within errors for general and specific case of (8) at $\sqrt{s_{NN}} = 5.52$ TeV (LHC) and $\sqrt{s_{NN}} = 39.0$ TeV (FCC) as well as for estimations obtained on basis of data sample (i) above.

TABLE IV: Estimations for observables based on fit results for the data sample (ii)

$\sqrt{s_{NN}}$, TeV	HBT parameter						
	λ	R_s^n	R_o^n	R_l^n	R_o/R_s	δ^n	V^n
5.52	0.25 ± 0.03	0.9 ± 0.2	0.8 ± 0.3	1.06 ± 0.16	0.9 ± 0.4	-0.2 ± 0.6	3.5 ± 1.6
	0.091 ± 0.004	0.792 ± 0.009	0.860 ± 0.010	1.099 ± 0.013	1.086 ± 0.018	0.11 ± 0.02	2.59 ± 0.07
39.0	0.22 ± 0.03	1.2 ± 0.4	0.9 ± 0.3	1.11 ± 0.16	0.7 ± 0.3	-0.7 ± 1.1	6 ± 4
	–	0.836 ± 0.011	0.883 ± 0.012	1.205 ± 0.015	1.06 ± 0.02	0.08 ± 0.03	3.17 ± 0.09

The energy dependencies for sets \mathcal{G}_m , $m = 1, 2$ of femtoscopy parameters with taking into account the scaling relation (7) and the high-statistics STAR data [12] demonstrate the reasonable agreement between values of parameters obtained for interactions of various ions (shown in Figs. 4 – 6). The observation confirms the suggestion [1] that normalized femtoscopy parameters allows to unite the study both symmetrical and asymmetrical nuclear-nuclear collisions in the framework of united approach. This qualitative suggestion is confirmed indirectly the recent study for pion femtoscopy in the collisions of the lightest nucleus (d) with heavy ion (Au) at RHIC. Estimations of space-time extent of the pion emission source in d+Au collisions at top RHIC energy [33] exhibit good agreement with values of corresponding parameters in Au+Au collisions and indicate on similarity in expansion dynamics in collisions of various systems (d+Au and Au+Au at RHIC, p+Pb and Pb+Pb at LHC). The scaling results for some radii indicate that hydrodynamic-like collective expansion is driven by final-state rescattering effects [33]. On the other hand the normalized femtoscopy parameters allow to get the common kinematic dependencies only without any additional information about possible general dynamic features in different collisions. Thus the hypothesis discussed above is qualitative only. The future quantitative theoretical and phenomenological studies are essential for verification of general features of soft stage dynamics for different collisions at high energies.

IV. SUMMARY

The following conclusions can be obtained by summarizing of the basic results of the present study.

Energy dependence is investigated for range of all experimentally available initial energies and for estimations of the main femtoscopy parameters from set \mathcal{G}_1 derived in the framework of Gauss approach as well as for set of important additional observables \mathcal{G}_2 . There are no the sharp changing of femtoscopy parameter values with increasing of $\sqrt{s_{NN}}$

in domain of collision energies $\sqrt{s_{NN}} \geq 5$ GeV. The estimation of emission duration of pion source is about $2 - 4$ fm/c for any energies under consideration. The energy dependence is almost flat both for emission duration and for δ^n parameter within large error bars. The indication on possible curve knee at $\sqrt{s_{NN}} \sim 10 - 20$ GeV obtained in STAR high-statistics data agree with other results in the framework of phase-I of beam energy scan program at RHIC. But additional precise measurements are crucially important at various $\sqrt{s_{NN}}$ in order to confirm this feature in energy dependence of additional femtoscopy parameters ($R_o/R_s, \Delta\tau, \delta^n$).

Analytic function is suggested for approximation of energy dependence of main HBT parameters. The fit curves demonstrate qualitative agreement with experimental data for λ at all available collision energies and for both absolute and normalized HBT radii in energy domain $\sqrt{s_{NN}} \geq 5$ GeV. Reasonable fit qualities are obtained for HBT radii at approximation of experimental points with total errors. Smooth curves calculated for energy dependence of set \mathcal{G}_2 of additional femtoscopy parameters agree reasonably with corresponding experimental data in the most cases. Estimations of femtoscopy observables are obtained on the basis of fit results for energies of the LHC and FCC project. As expected for multi-TeV domain the pion source will be characterized by decreased chaoticity parameter, linear sizes about $8.5 - 9.5$ fm in longitudinal direction and $7 - 8$ fm in transverse plane, volume of about 10^4 fm³.

-
- [1] V. A. Okorokov, arXiv: 1312.4269 [nucl-ex]. 2013.
 - [2] Yu. Sinyukov, In "Hot hadronic matter: theory and experiment". NATO ASI Series B346, 309 (1995). Plenum Publishing Corp., New York. Eds. J. Letessier, H. G. Gutbrod, J. Rafelski.
 - [3] V. A. Okorokov, *Strange particle femtoscopy in relativistic heavy ion collisions: experimental overview*. Proceedings of the XVIII International Baldin Seminar on High Energy Physics Problems. Dubna. V. II, 2008. P. 101. Eds. by A.N. Sissakian, V.V. Burov, A.I. Malakhov.
 - [4] S. Pratt, Phys. Rev. D33, 1314 (1986).
 - [5] G. F. Bertsch, M. Gong, M. Tohyama, Phys. Rev. C37, 1896 (1988).
 - [6] U. A. Wiedemann, U. Heinz, Phys. Rep. 319, 145 (1999).
 - [7] V. A. Okorokov, E. V. Sandrakova, *Fractals in fundamental physics. Fractal properties of multiparticle production and topology of sample*. MEPhI, Moscow, 2009.
 - [8] G. F. Bertsch, Nucl. Phys. A498, 173c (1989).
 - [9] S. Pratt, T. Csörgő, J. Zimányi, Phys. Rev. C42, 2646 (1990).
 - [10] L. Valentin, *Subatomic physics: nuclei and particles*. V. I. Ermann, Paris, 1982.
 - [11] K. N. Mukhin, *Experimental nuclear physics*. V. I. Energoatomizdat, Moscow, 1983.
 - [12] L. Adamczyk *et al.*, arXiv: 1403.4972 [nucl-ex]. 2014.
 - [13] J. Adams *et al.*, Phys. Rev. C71, 044906 (2005).
 - [14] F. Retière, M. A. Lisa, Phys. Rev. C70, 044907 (2007).
 - [15] E. Mount *et al.*, Phys. Rev. C84, 014908 (2011).
 - [16] W. Broniowski, Phys. Rev. Lett. 101, 022301 (2008).
 - [17] S. Pratt, Phys. Rev. Lett. 102, 232301 (2009).
 - [18] Iu. A. Karpenko, Yu. M. Sinyukov, Phys. Lett. B688, 50 (2010).
 - [19] Iu. A. Karpenko, Yu. M. Sinyukov, Phys. Rev. C81, 054903 (2010).
 - [20] K. Werner *et al.*, Phys. Rev. C82, 044904 (2010).
 - [21] P. Bozek, Phys. Rev. C83, 044910 (2011).
 - [22] F. Antinori *et al.*, J. Phys. G: Nucl. Part. Phys. 27, 2325 (2001).
 - [23] V. A. Okorokov, *Azimuthal anisotropy and fundamental symmetries in QCD matter at RHIC*. Proceedings of the XIII International Conference on Selected Problems of Modern Physics. Dubna. E1,2-2009-36, 2009. P. 201. Eds. B.M. Barbashov, S.M. Eliseev; arXiv: 0809.3130 [nucl-ex].
 - [24] G. Alexander, I. Ben Mordechai, J. Phys. G: Nucl. Part. Phys. 40, 125101 (2013).
 - [25] H. Heiselberg, A. P. Visher, Eur. Phys. J. C1, 593 (1998).
 - [26] L. McLerran, S. S. Padula, arXiv: nucl-th/0205028. 2002.
 - [27] L. Adamczyk *et al.*, Phys. Rev. C88, 014902 (2013).
 - [28] L. Adamczyk *et al.*, Phys. Rev. Lett. 110, 142301 (2013).
 - [29] L. Adamczyk *et al.*, Phys. Rev. Lett. 112, 032302 (2014).
 - [30] L. Adamczyk *et al.*, Phys. Rev. Lett. 112, 162301 (2014).
 - [31] L. Adamczyk *et al.*, Phys. Rev. Lett. 113, 052302 (2014).
 - [32] L. Adamczyk *et al.*, Phys. Rev. Lett. 113, 092301 (2014).
 - [33] A. Adare *et al.*, Phys. Rev. Lett. 112, 222301 (2014).

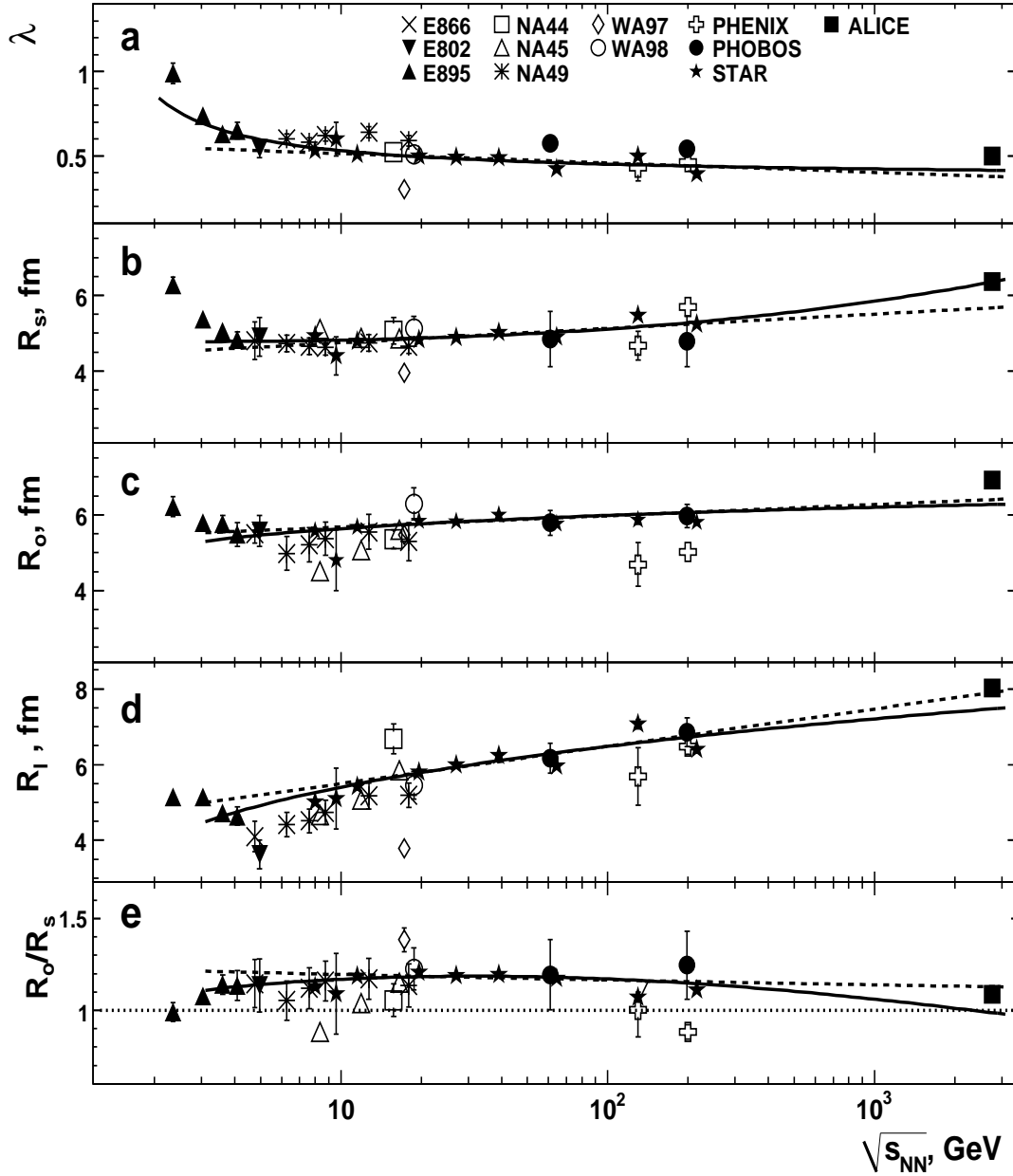


FIG. 1: Dependence of chaoticity parameter (a), HBT-radii (b – d) and ratio R_o/R_s (e) on initial energy for central heavy ion Au+Au, Au+Pb, Pb+Pb collisions at midrapidity and $\langle k_{\perp} \rangle \simeq 0.2 \text{ GeV}/c$ [1, 12]. Experimental results are demonstrated for pairs of π^- mesons (in cases of ALICE, STAR at $\sqrt{s_{NN}} = 7.7 - 62.4$ and 200 GeV – for $\pi^{\pm}\pi^{\pm}$ pairs) and for standard Coulomb correction $P_C^{(1)}(q)$ (in cases of ALICE, NA44, NA45, PHOBOS and STAR at $\sqrt{s_{NN}} = 7.7, 11.5 - 62.4$ and 200 GeV – for correction $P_C^{(3)}$). Statistical errors are shown (for NA44 – total uncertainties). The solid lines (a – d) correspond to the fits by function (8) and dashed lines – to the fits by specific case $G_1^i \propto \ln \varepsilon$, $i = 1 - 4$. Fitted data samples for λ (a) and for R_l (d) do not include the point of the WA97 experiment [22] while the fits for transverse HBT radii (b, c) are shown for samples with point from [22]. Smooth solid and dashed curves at (e) correspond to the ratio R_o/R_s calculated from fit results for R_s and R_o , dotted line is the level $R_o/R_s = 1$.

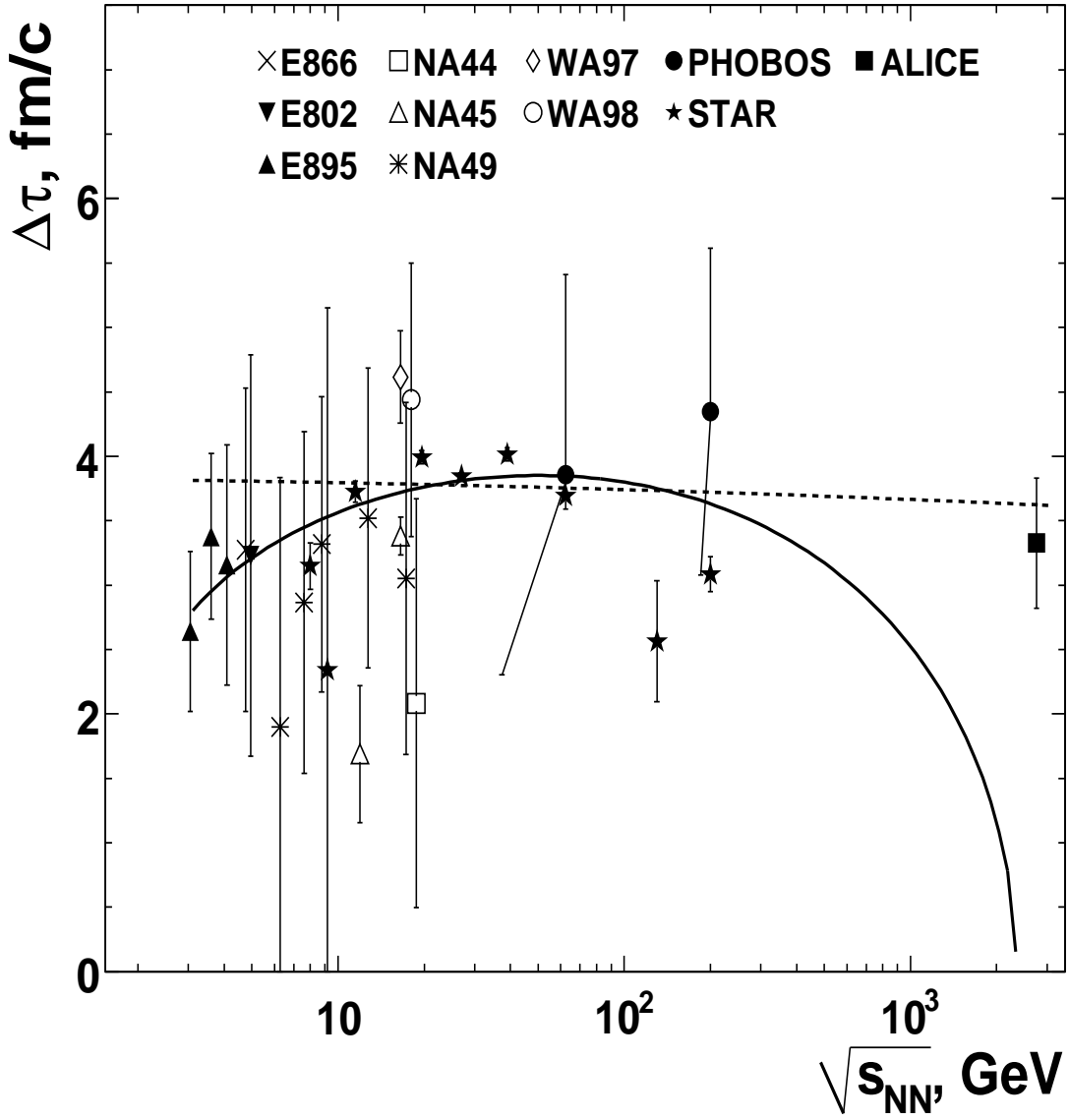


FIG. 2: Energy dependence of emission duration for secondary charged pions in central heavy ion collisions Au+Au, Au+Pb, Pb+Pb in midrapidity region and at $\langle k_{\perp} \rangle \simeq 0.2$ GeV/c. Experimental results are shown for the same particle types and Coulomb corrections as well as in Fig. 1. Error bars are only statistical (for NA44 – total uncertainties). Smooth curves are derived from (6) and fit results for R_s , R_o without the point of the WA97 experiment [22]. The solid line corresponds to the fits of HBT radii by function (8) and dashed line – to the fits by specific case $R_i \propto \ln \varepsilon$, $i = s, o$.

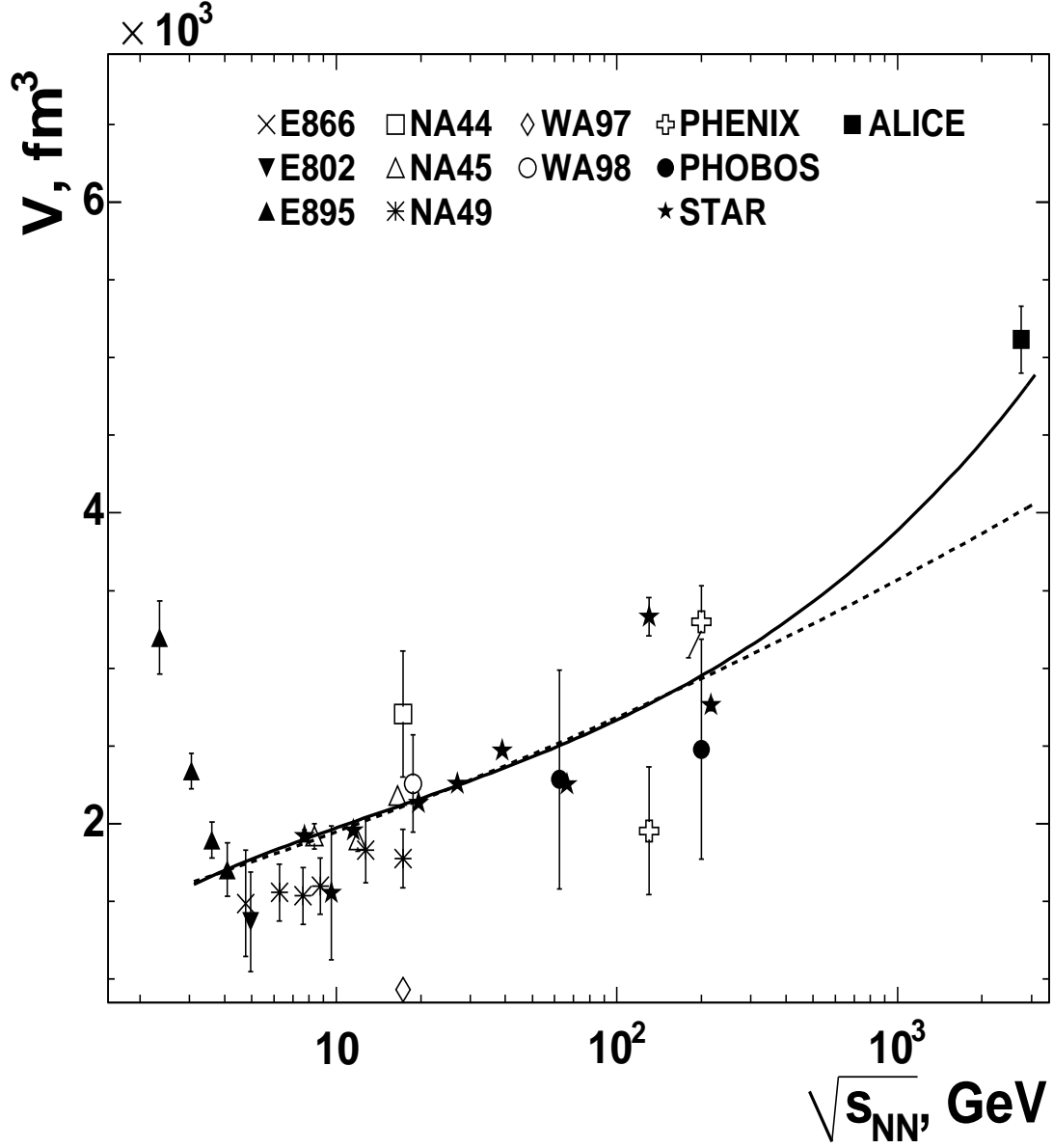


FIG. 3: Energy dependence of volume of emission region at freeze-out for secondary charged pions in central heavy ion collisions Au+Au, Au+Pb, Pb+Pb in midrapidity region and at $\langle k_{\perp} \rangle \simeq 0.2$ GeV/c. The equation (4) is used for calculation of volume values. Experimental results are shown for the same particle types and Coulomb corrections as well as in Fig. 1. Error bars are only statistical (for NA44 – total uncertainties). Smooth curves are derived from (4) and fit results for R_s , R_l with taking into account the point of the WA97 experiment [22]. The solid line corresponds to the fits of HBT radii by function (8) and dashed line – to the fits by specific case $R_i \propto \ln \varepsilon$, $i = s, l$.

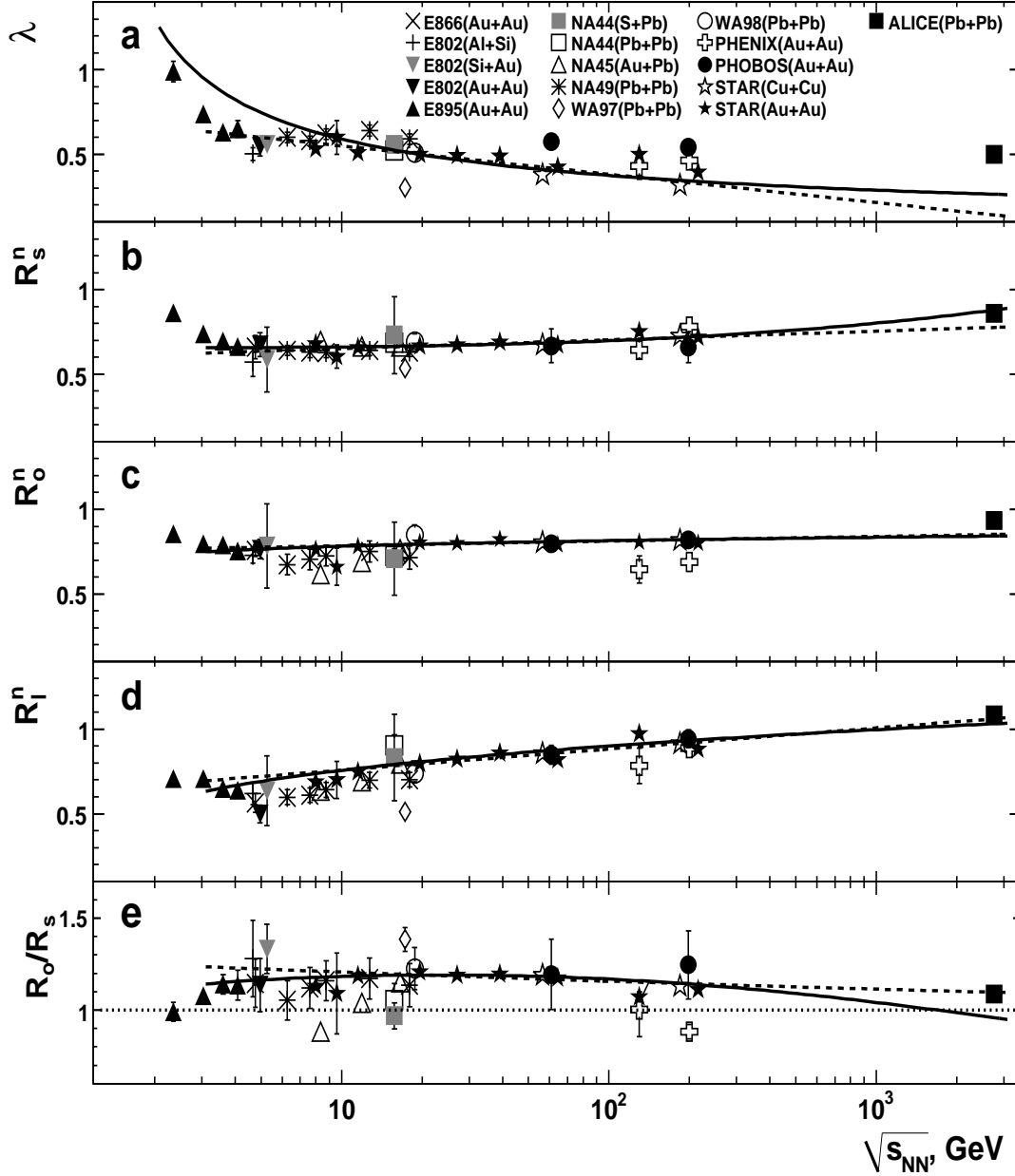


FIG. 4: Energy dependence of λ parameter (a), normalized HBT-radii (b – d) and ratio R_o/R_s (e) in various nuclear-nuclear collisions at $\langle k_\perp \rangle \simeq 0.2$ GeV/c [1, 12]. Experimental results are shown for central collisions (for minimum bias event in the case of E802 for Al+Si), for pairs of π^- mesons (in cases ALICE and STAR both for Cu+Cu and for Au+Au at $\sqrt{s_{NN}} = 7.7 - 62.4$ and 200 GeV – for $\pi^\pm\pi^\pm$ pairs, E802 for Al+Si, NA44 for S+Pb – for pairs of π^+ mesons) and for standard Coulomb correction $P_C^{(1)}(q)$ (in cases ALICE, NA44, NA45, PHOBOS, STAR both for Cu+Cu and for Au+Au at $\sqrt{s_{NN}} = 7.7, 11.5 - 62.4$ and 200 GeV – for correction $P_C^{(3)}$). Statistical errors are shown (for NA44 – total uncertainties). The solid lines (a – d) correspond to the fits by function (8) and dashed lines – to the fits by specific case of (8) at fixed $a_3 = 1.0$. Smooth solid and dashed curves at (e) correspond to the ratio R_o/R_s calculated from fit results for R_s^n and R_o^n , dotted line is the level $R_o/R_s = 1$.

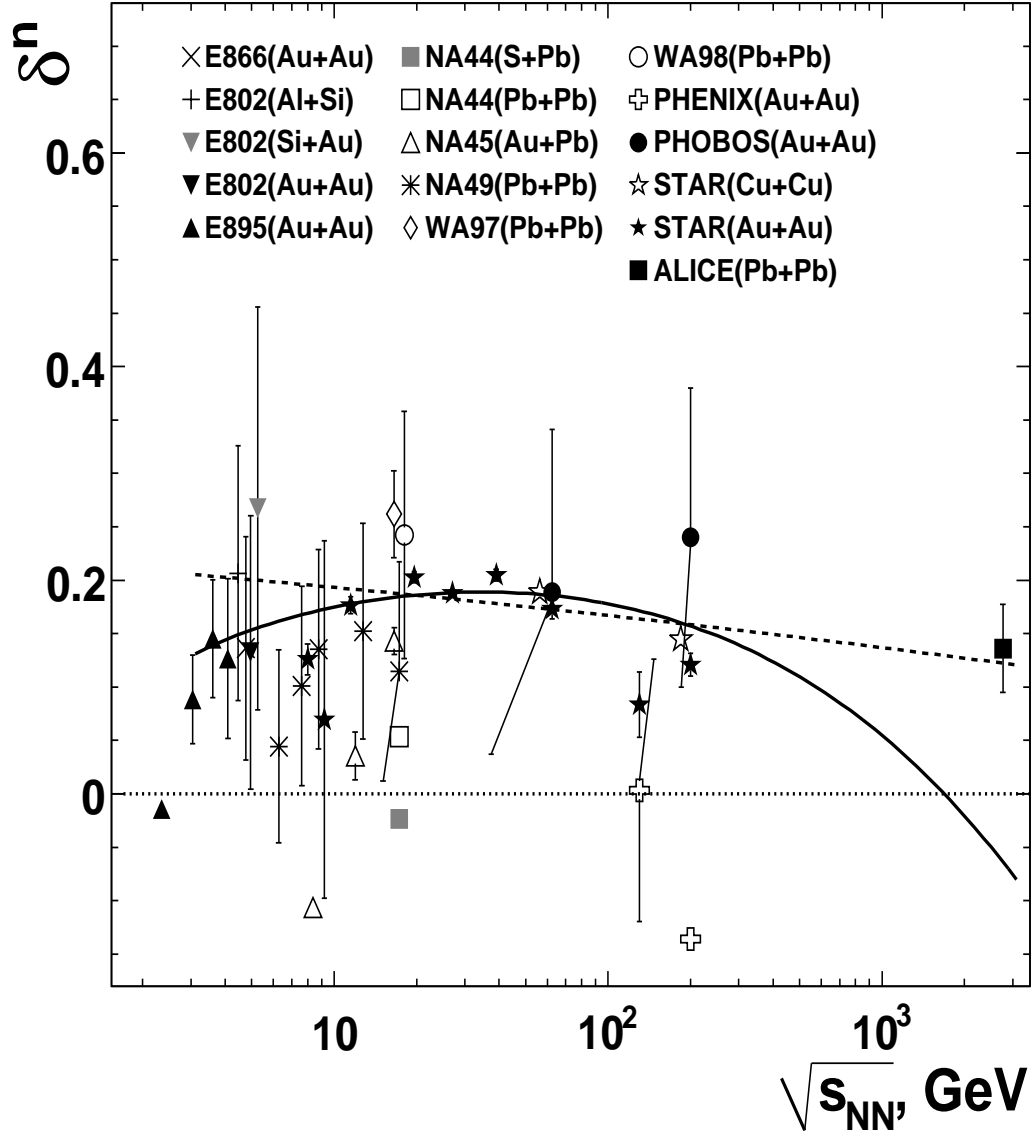


FIG. 5: Dependence of scaled difference of squares of transverse radii on beam energy for emission region of secondary charged pion in various nuclear-nuclear collisions at $\langle k_{\perp} \rangle \simeq 0.2$ GeV/ c . Experimental results are shown for the same particle types and Coulomb corrections as well as in Fig. 4. Error bars are only statistical (for NA44 – total uncertainties). Dotted line is the level $\delta^n = 0$. Smooth curves are derived from (7) and fit results for R_s^n , R_o^n . The solid line corresponds to the fits of normalized HBT radii by function (8) and dashed line – to the fits by specific case $R_i^n \propto \ln \varepsilon$, $i = s, o$.

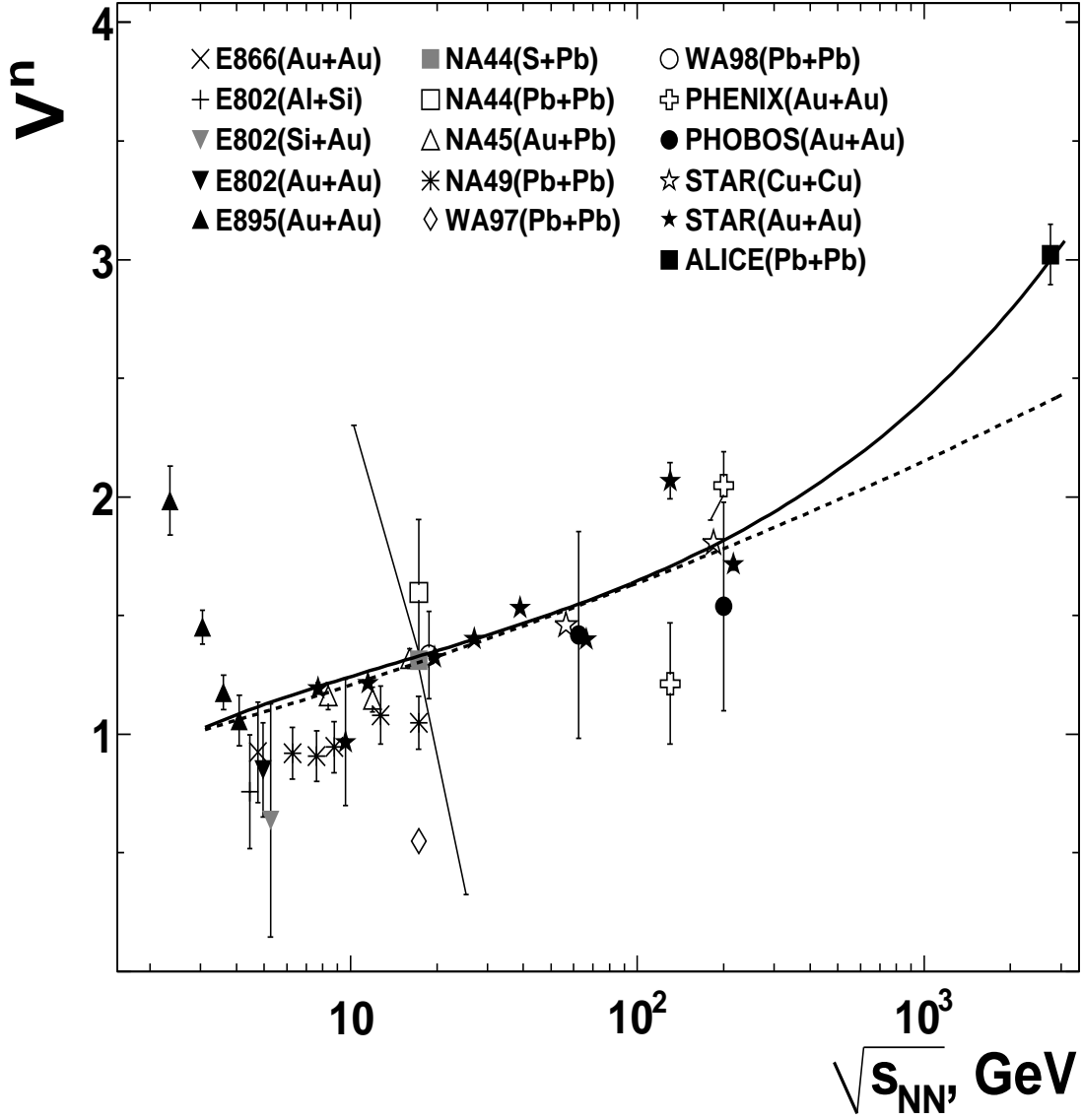


FIG. 6: Energy dependence of normalized volume of emission region at freeze-out for secondary charged pions in various nuclear-nuclear collisions at $\langle k_{\perp} \rangle \simeq 0.2$ GeV/ c . The equation (4) is used for calculation of volume values. Experimental results are shown for the same collision, particle and Coulomb correction types as well as in Fig. 4. Error bars are only statistical (for NA44 – total uncertainties). Smooth curves are derived from (4) and fit results for R_s^n, R_l^n . The solid line corresponds to the fits of normalized HBT radii by function (8) and dashed line – to the fits by specific case $R_i^n \propto \ln \varepsilon$, $i = s, l$.